Near-field Optical Patterning on Chloromethylated Polyimide

J.-B. Kim*, S.-J. Na
Department of Mechanical Eng, KAIST
373-1 Guseong-dong, Yuseong-gu, Daejeon, Korea
W.-S. Chang, M.-J. Choi
Nanoprocess Group, KIMM
171 Jang-dong, Yuseong-gu, Daejeon, Korea

Near-field scanning optical microscopy(NSOM) coupled with laser is used in nano-scale processing to make nano-scale dots or nano-scale structure. Nano-sclae processing using NSOM coupled with laser can be applied to photo- chemical etching process on crstalline silicon, to additive processes on some polymers, to subtraction processes on SAMs and other polymers. And it can be used to change material's optical properties in nano-scale geometry. As above, nano-scale processing using NSOM coupled with laser has an advantage that it can be applied to various processes. In this work, by using NSOM coupled with 266nm UV laser, nano-scale patterns were fabricated on chloromethylated polyimide(CMPI) films coated on silicon wafer. CMPI undergoes a fast photolysis under UV light. So, in the case of pattern fabrication on CMPI it is possible to fabricate patterns without development process. Possibilities for SMPI to be applied to nano-scale patterns fabrication were demonstrated. Compared to usual lithographic processes, the process proposed in this work is simple because development, one of steps to fabricate nano-scale patterns, is not needed. And the finite-difference-time-domain (FDTD) method was employed to simulate the energy intensity distribution in the near-field. The simulation was executed for NSOM tip and UV laser. The influence of aperture size and tip-sample distance on the resolution of the lithographic process is discussed from the simulation results. Comparison of some simulation results with corresponding experimental results could confirm the validity of the simulation model proposed.

Key Words : Near-Field, Pattem Fabrication, SPM Lithography

1. Introduction

The demand for high performance, integrity, and miniaturization in the area of electronic, mechanical, and bionic devices has led to heightened interest in the fabrication of nanostructures on surfaces (Lee et al., 2004). Since Binning et al.(1982) first developed the scanning probe microscope (SPM) in 1982; SPM has been used primarily to obtain topography and electronic surface maps. At present, SPM is also being used to fabricate patterns and structures in nano-scale. Among several methods of SPM lithography, especially NSOM lithography has an advantage that it can be applied to various materials (Riehn et al., 2003; Landraud et al., 2001; Naber et al., 2000; Wysocki et al., 2004; Sun and Leggett, 2002).

Figure 1 shows a typical photolithographic process. As described in this figure, eight steps are needed to make patterns, and their resolutions are limited by diffraction of incident light. However, probe lithography processes, as noted by many previous researchers, do not require mask fabri-

* Corresponding Author,
E-mail : jkim@alpa.kaist.ac.kr
TEL : +82-42-869-3256; **FAX** : +82-42-869-3210
Department of Mechanical Eng, KAIST 373-1 Guseong-dong, Yuseong-gu, Daejeon, Korea. (Manuscript **Received** January 25, 2005; **Revised** May 13, 2005)

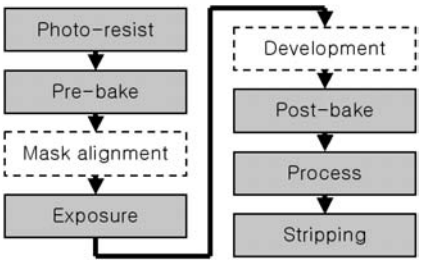

Fig. 1 Typical photo-lithographic process

cation and alignment, because patterns are fabricated by direct writing. Furthermore, NSOM lithography makes it possible to make nano-scale patterns that overcome the diffraction limit. CMPI, synthesized by Lee et al.(Zhang et al., 2003), undergoes rapid photolysis under UV light. Hence, in the case of pattern fabrication on CMPI, it is possible to fabricate patterns without a development process. Compared to usual lithographic processes, this process, which uses CMPI as photo-resist layers, is simple, because development is not needed. In this work, CMPI is applied to nano-scale patterns fabrication to demonstrate its potential utility in this field. Further, the finite-difference-time-domain (FDTD) method was employed to simulate the energy intensity distribution in the near-field. The simulation was executed for an NSOM tip, UV laser, and CMPI as a target sample.

2. Experiment

2.1 Experimental setup

Figure 2 shows the configuration of the experimental equipment. An NSOM/SPM-100 manufactured by NANONICS IMAGING Ltd. was used for control of tip-sample distance and PZT stages. As the optical energy source, a 4th-harmonic Nd : YAG laser by Big Sky Laser was used and light at a wavelength of 266 nm was emitted by pulse mode. A half-wave plate and a polarizing beam splitter were used to adjust the laser power, and a shutter was used to control exposure time of light.

CMPI was synthesized and provided by Lee et al.(Zhang et al., 2003), and samples were prepared by spin-coating and curing. CMPI films were coated on a silicon wafer with thickness around 70 nm. The temperature of the sample was maintained at 100℃ for 10 minutes to procure, and then at 200℃ for 60 minutes to cure.

2.2 Experimental results

Figure 3 shows the holes array fabricated by illumination. Illumination was conducted through a probe having a diameter of 1 μm. Fig 3 (a) shows an image of the array by an optical microscope, and Fig 3 (b) is an image by AFM. Laser power injected into the fiber was 90 μW. Exposure time at each point was 100 ms, and the distance between each point was 2 μm. As shown in Fig. 3, holes are fabricated on the surface uniformly, and the diameter of each hole is approximately 1 μm ; this value is similar to the diameter of the probe. The depth of holes is between 50 μm and 60 μm. We have deliberately omitted several dots in the third line in order to illustrate that arbitrary sequences can be fabricated. And therefore corresponding holes were not fabricated.

Figure 4 shows an AFM image of the holes array fabricated by illumination. Illumination

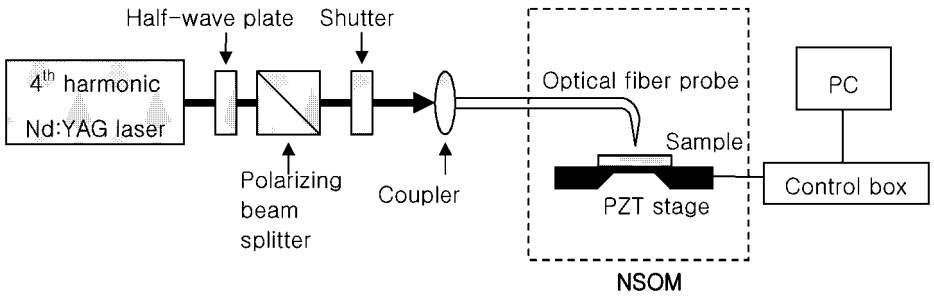

Fig. 2 Experimental set up

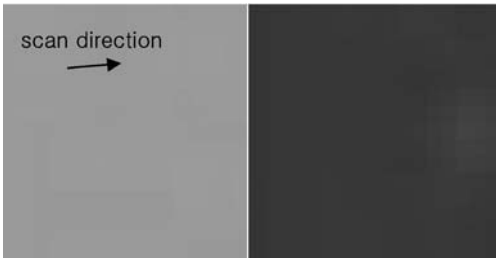

(a) (b)

Fig. 3 Image of fabricated holes array (aperture diameter=1 μm). (a) optical microscope image, (b) AFM image

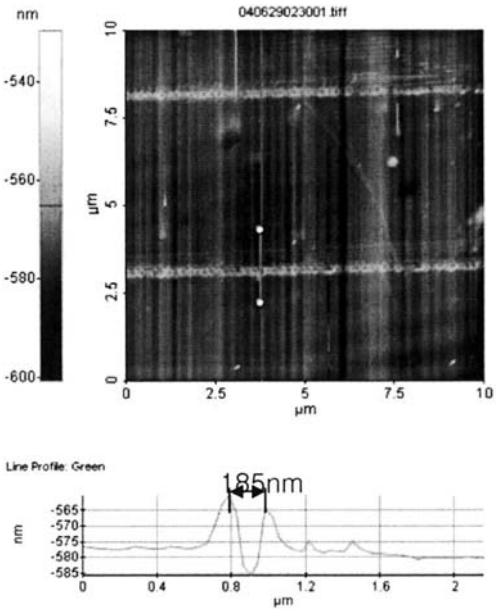

Fig. 4 AFM image of the holes array fabricated (aperture diameter=200nm)

was achieved through a probe having a diameter of 200 nm. In this experiment, uniform holes were also obtained. Laser power injected into the fiber was 200 μW. Exposure time at each point was 500 ms, and the distance between each point was 300 nm. As shown in the topology image provided in Fig 4, the hole is shaped like a crater ; the boundary protrudes and the center is depressed. The diameter of the protruding boundary is approximately 185 nm and the diameter of the depressed area, the height of which is lower than the non-illuminated region, is about 100 nm. The mechanism of the protruding boundary production has not been clearly identified. However, it is believed that the surface of the sample protrudes when the intensity of illuminating light is below the threshold value for photolysis. The height of protrusion is about 10 nm, and the center of the hole is depressed by as much as 10 nm relative to non-illuminated regions.

3. Simulation

To study the influence of experimental variables on the size of hole fabricated, simulations were executed for energy intensity distribution in the near-field. To execute the simulation, commercial code XFDTD-pro based on finite-difference- time-domain (FDTD) algorithm is used. The FDTD algorithm is used and studied as a tool to simulate electromagnetic field distribution in nano-scale. The simulation was executed for an NSOM tip, UV laser, and a sample in 3-dimensions.

Details of the models used in the simulation are as follows. Thickness of the sample film was defined as 70 nm. The tip angle of the probe was 35° ; and this value was based on the shape of the probe used in the experiments. Light at a wavelength of 266 nm was used as incident light. Two diameters of probe aperture and three tip-sample distances were used for the simulations. The probe diameters were 100 nm and 200 nm, and tip-sample distances considered in the simulation were 5 nm, 30 nm, and 50 nm.

Figure 5 shows the simulation results, which are a normalized energy intensity distribution at the sample surface. Figs. 5(a), (c), (e) are the results for the cases, aperture diameters are same value, 100 nm, and tip-sample distance is each 5 nm, 30 nm, and 50 nm. Figs. 5(b), (d), (f) are the results for the cases, all aperture diameters are 200 nm and tip-sample distance is each 5 nm, 30 nm, 50 nm. To compare the energy intensity distribution of each case, each result is normalized by dividing by its maximum energy intensity value, and then expressed graphically. In the cases where the aperture diameter is 200 nm, the energy intensity distribution is fairly circular, whereas for aperture diameters of 100 nm, the energy intensity

distribution is peanut-shaped, with a center that is narrower than other parts. This phenomenon is caused by local electromagnetic field enhancement produced at points where the polarization direction and boundary of an aperture, of which the diameter is much smaller than the wavelength of incident light, meet perpendicularly (Jung, 2000). In the cases of Fig. 5(b), (d), and (f), the

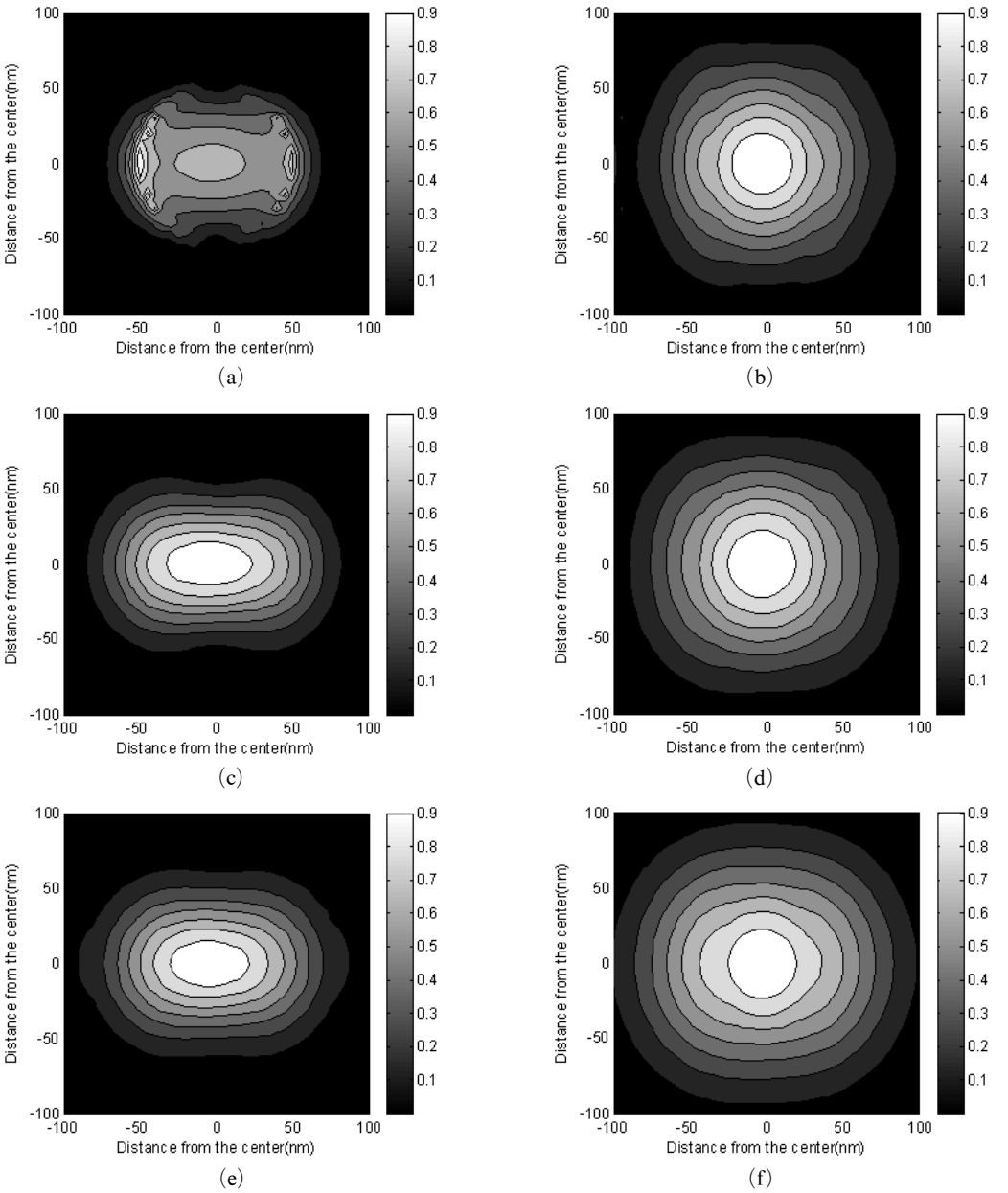

Fig. 5 Simulation results : normalized energy intensity distribution. (a) aperture diameter=100 nm, tip-sample distance=5 nm, (b) aperture diameter=200 nm, tip-sample distance=5 nm, (c) aperture diameter=100 nm, tip-sample distance=30 nm, (d) aperture diameter=200 nm, tip-sample distance=30 nm, (e) aperture diameter=100 nm, tip-sample distance=50 nm, (f) aperture diameter=200 nm, tip-sample distance=50 nm.

aperture diameter, i.e., 200 nm, is smaller than 266 nm, the wavelength of incident light. However, when the aperture diameter is similar to the wavelength of incident light, local electromagnetic field enhancement is very weak (Kim and Na, 2004). In cases where the aperture diameter is 100 nm, the length of the spots in perpendicular direction to the polarization direction is similar to the aperture diameter ; however, the length of the spots in parallel direction to the polarization direction is 1.5-1.8 times as large as the aperture diameter. On the other hand, in cases where the aperture diameter is 200 nm, the length of the spots is similar to the aperture diameter, regardless of polarization direction. In the simulation result energy intensity distribution becomes broader with tip-sample distance, regardless of aperture diameter. This is due to diffraction on the aperture. From this result, it is verified that to obtain a smaller spot than spot to be limited by the diffraction limit, tip-sample distance must be as small as possible.

The graph in Fig. 6 shows the maximum values of energy intensities for each case. This serves to estimate the transmission efficiency of the probe and degree of energy intensity concentration at the sample surface. The maximum values of the cases where the aperture diameter is 200 nm are larger than the others, and the maximum values decrease with respect to tip-sample distance, regardless of aperture diameter. From this result, the transmission efficiency of the probe having an aperture diameter of 200 nm is higher than the transmission efficiency of the probe having an aperture diameter of 100 nm. Further, as the tip-sample distance is decreased, the concentration of energy intensity at the sample surface becomes denser. This result corresponds to the results given in Fig. 5.

Figure 7 shows the energy intensity distribution at a vertical plane to the sample surface and cross-section of the pattern fabricated in Fig. 4. The diameter of the probe aperture was 200 nm, and the tip-sample distance was 30 nm. These conditions correspond with those for the experiment illustrated in Fig. 4. In the figure, the hori zontal axis reflects the distance from the center,

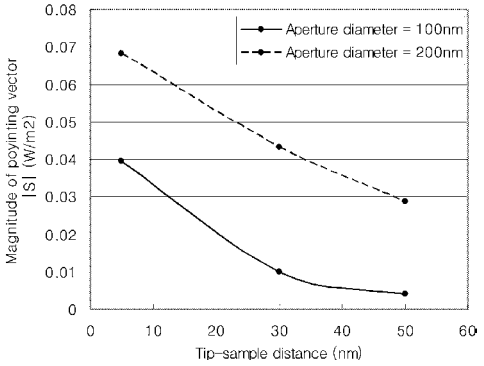

Fig. 6 Maximum values of energy intensities

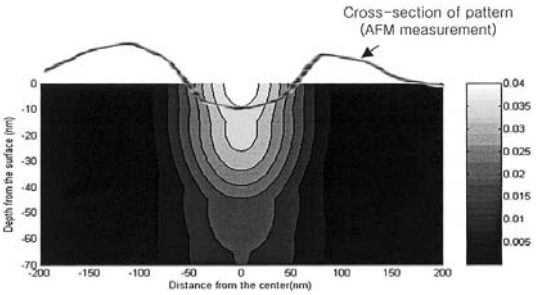

Fig. 7 Energy intensity distribution calculated at a vertical plane to the sample surface. (aperture diameter=200 nm, tip-sample distance=30 nm), and cross-section of pattern (measured by AFM)

and the vertical axis is the depth from the surface. In the experiment, the diameter of depressed area was approximately 110 nm, and the depth was about 10 nm. However, in the simulation, a surface layer of constant intensity, of which the diameter is about 110 nm at the sample surface, reaches a depth of 45 nm. Compared to the simulation results, the depth of holes fabricated in the experiment is shallow. The reason for this is believed to be that the model used in the simulation does not consider the energy required for photolysis of CMPI. Thus, additional work is required to enable a more quantitative prediction of size and shape of holes.

4. Conclusion

In this work, possibilities for application of CMPI to nano-scale patterns fabrication were

demonstrated. Size of patterns fabricated were about 110-185 nm. It was shown that arbitrary patterns of CMPI could be fabricated. In addition, a study on the influence of experimental variables on the size of fabricated holes was conducted through simulations.

Acknowledgment

This research has been supported by a grant (No. M102KN010006-04K1401-00612) from the Center for Nanoscale Mechatronics & Manufacturing of the 21st Century Frontier Research Program.

References

Binning, G., Rohrer, H., Gerber, Ch. and Weibel, E., 1982, "Surface Studies by Scanning Tunneling Microscopy," Physical review letters, Vol. 49, pp. 57～61.

Jung, S. T., 2000, "High-power Near-field Probes and Their Applications to Optical Recording," *Ph.D. Thesis, KAIST*, pp. 23～42.

Kim, J.-B. and Na, S.-J., 2004, "Sub-micro Machining by using Near Field Effect of Femtosecond Laser," *in Proceedings of the 2004 spring annual meeting of Korean welding society*, pp. 97～99

Landraud, N., Peretti, J., Chaput, F., Lampel, G., Boliot, J.-P., Lahlil, K. and Safarov, V. I., 2001, "Near-field Optical Patterning on Azo-hybrid Sol-gel Films," *Applied physics letters*, Vol. 79, No. 27, pp. 4562～4564.

Lee, S., Kim, J., Shin, W. S., Lee, H.-J., Koo, S. and Lee, H., 2004, "Fabrication of Nanostructures using Scanning Probe Microscope Lithography," *Materials science and engineering C*, Vol. 24, pp. 3～9.

Naber, A., Dziomba, T., Fischer, U. C., Mas, H.-J. and Fuchs, H., 2000, "Photopatterning of a Monomolecular dy Film by Means of Scanning Near-field Optical Microscopy," *Applied physics*, Vol. A70, pp. 227～230.

Riehn, R., Charas, A. and Morgado, J., 2003, "Near-field Optical Lithography of a Conjugate Polymer," *Applied physics letters*, Vol. 82, No. 4, pp. 526～528.

Sun, S. and Leggett, G. J., 2002, "Generation of Nanostructures by Scanning Near-field Photolithography of Self-assembled Monolayers and Wet Chemical Etching," *Nano letters*, Vol. 2, No. 11, pp. 1223～1227.

Wysocki, G., Heitz, J. and Bauerle, D., 2004, "Near-field Optical Nanopatterning of Crystalline Silicon," *Applied physics letters*, Vol. 84, No. 12, pp. 2025～2027.

Zhang, A., Li, X., Nah, C., Hwang, K. and Lee, M.-H., 2003, "Facile Modifications of a Polyimide Via Chloromethylation. I. Novel Synthesis of a New Photosensitive Polyimide," *Journal of polymer science : part A : polymer chemistry*, Vol. 41, pp. 22～29.